IX International Conference on Particle-Based Methods
PARTICLES 2025
J. Bonet, M. Cremonesi, A. Franci, A. Gil (Eds)

OPTIMIZING PERIDYNAMIC MICROPARAMETERS FOR ACCURATE REPRESENTATION OF ELASTICITY, PLASTICITY, AND SHEAR LOCALIZATION IN GEOMATERIALS

SOURABH NANDWAL * **AND SUMEET KUMAR SINHA** *

* Department of Civil and Environmental Engineering
Indian Institution of Technology Delhi
Hauz Khas, New Delhi-110016, India
e-mail: sourabh.nandwal@civil.iitd.ac.in, sksinha@civil.iitd.ac.in

Key words: Peridynamic, Geomaterials, Elastic Stiffness, Shear Band.

Abstract. Geomaterials exhibit complex failure mechanisms characterized by strain localization and discontinuities (such as micro-crack formation and propagation), posing substantial challenges in their numerical modelling using the continuum-based methods. These limitations are typically addressed through algorithmic interventions or by using a non-local formulation. Peridynamic is one such method that inherently overcomes these limitations by replacing the partial differentials with non-local integral equations, enabling material points to interact with neighbouring points within a defined horizon. Similar to other numerical approaches, the application of peridynamic in geomechanics necessitates precise calibration of elastic parameters, as they play a crucial role in governing the plastic behavior of geomaterials. In this context, the present investigation studied the optimization of non-ordinary state-based peridynamic formulations using a geomaterial test specimen with a 1:2 aspect ratio under compression to evaluate the influence of critical numerical parameters, namely horizon size and material points discretization, on the accuracy of predicted elastic modulus. The results highlighted the necessity of selecting optimal combinations of mesh density and horizon size to achieve convergence toward input elastic properties. Furthermore, the obtained optimized parameters were used to simulate a series of plane strain compression tests on geomaterials to gain insight into plastic deformation and shear band formation. The study affirmed that parameter calibration is fundamental for accurately capturing both elastic and plastic behaviors of geomaterials. This calibrated model can offer significant potential for modelling failure surfaces below foundations, behind a retaining wall, and on a slope.

1 INTRODUCTION

Geomaterial such as soil is an inherently heterogeneous material that exhibits complex failure mechanisms characterized by strain localization and discontinuities[1, 2]. To model these complex mechanisms, the classical continuum-based models, such as the finite element method (FEM), encounter significant limitations due to high mesh dependency and the absence of a non-local zone, which is essential for capturing the non-local behavior of geomaterials[3]. Additionally, FEM formulations based on partial differential equations face convergence difficulties at discontinuities[3]. To address these limitations, Silling[4] proposed the

peridynamic (PD) model. PD represents a non-local continuum model that replaces the partial differentials with non-local integral equations, enabling material points to interact with neighbouring points within a defined horizon[4]. The peridynamic theory encompasses three distinct formulations: bond-based peridynamic (BB-PD)[4], ordinary state-based peridynamic (OSB-PD)[5], and non-ordinary state-based peridynamic (NOSB-PD)[5, 6]. In BB-PD, the force density depends only on the individual bond, whereas in OSB-PD and NOSB-PD, it is influenced by all bonds connected to the interacting material points[5]. Additionally, the OSB-PD requires collinearity between the bond force and bond vectors; however, this constraint is released in the NOSB-PD, making it capable of modelling complex mechanical behavior of geomaterials[1, 5, 7].

The NOSB-PD framework enables the incorporation of classical continuum constitutive models into peridynamic theory, whereas the constrained formulations of BB-PD and OSB-PD cannot handle such integrations[5, 6]. Similar to other numerical approaches (FEM, material point method, and discrete element method), the application of peridynamic in geomechanics necessitates precise calibration of elastic parameters, as they play a crucial role in governing the plastic behavior of geomaterials[8-13]. This calibration process necessitates optimization of PD microparameters, including horizon and material points discretization.

Several studies have investigated the convergence of peridynamics microparameters towards the elastic properties[8, 9]. Bobaru et al.[14] examined the numerical convergence of peridynamic to classical elasticity. Liu and Hong[15] performed horizon optimization to achieve convergence of the linear elastic modulus using the BB-PD frameworks. Moreover, for the elastoplastic behavior in geomaterials, Menon and Song[16] simulated the shear bands in unsaturated clays, while Song and Khalili[1] investigated the regularization effect of the horizon on strain localization. However, most microparameter optimization studies for elastic modulus were conducted using BB-PD[10, 11]. While peridynamic models for geomaterials typically utilize Drucker-Prager criteria to analyze strain localization, this behavior remains unexplored within the von Mises yield criterion in the peridynamic framework[1, 12].

This paper implements the elastoplastic constitutive model with the von Mises yield criterion in NOSB-PD (1) to calibrate the elastic modulus through systematic microparameter optimization, and (2) to analyze the regularization effect of the horizon on shear band formations and on shear band width evolution. Finally, the influence of loading conditions and specimen size on shear band development patterns was investigated.

2 NON-ORDINARY STATE BASED (NOSB) PERIDYNAMIC FRAMEWORK

Peridynamic (PD) is a continuum theory proposed by Silling in 2001[4], which replaces the partial differential equations of classical continuum mechanics with non-local integral equations, enabling material points to interact with neighbouring points within a defined horizon (δ), as shown in Figure 1. Let x and x' be two material point coordinates in the initial configuration and y and y' are the spatial coordinates in the current configuration, respectively. $\xi = x' - x$ is the relative distance vector between x and x', defined as a bond[4]. In PD, material points only interact within δ, where the family of x is defined as $H_x = \{\xi \mid ||x' - x|| < \delta$. In the current configuration, u and u' are the displacement vectors for x and x', respectively; $\eta = u' - u$ is the relative displacement vector for the bond and $y\langle\xi\rangle = y' - y = \xi + \eta$ is the deformation state[4].

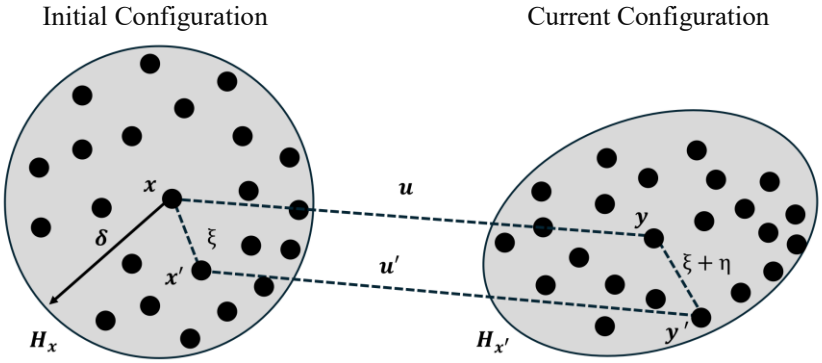

Figure 1: Illustration of peridynamic

The NOSB-PD governing equation for a material point x can be written as

$$\rho\ddot{\boldsymbol{u}} = \int_{H_x} (\boldsymbol{T}[\boldsymbol{x}]\langle\xi\rangle - \boldsymbol{T}[\boldsymbol{x}']\langle-\xi\rangle) dV_{x'} + \boldsymbol{b}[\boldsymbol{x}] \tag{1}$$

where $\boldsymbol{T}[\boldsymbol{x}]\langle\xi\rangle$ and $\boldsymbol{T}[\boldsymbol{x}']\langle-\xi\rangle$ are the force state at x and x', respectively, $dV_{x'}$ is the volume of a material point x', and $\boldsymbol{b}$ is the body force density[6].

To incorporate the classical constitutive models into NOSB PD, a constitutive correspondence formulation can be adopted[5]. This formulation employs a non-local approximation of the deformation gradient tensor, $\boldsymbol{F}$, given as

$$\boldsymbol{F} = \left[\int_{H_x} \omega\langle|\xi|\rangle(\boldsymbol{Y} \otimes \xi\,) dV_{x'}\right] \boldsymbol{K}^{-1} \tag{2}$$

$$\boldsymbol{K} = \int_{H_x} \omega\langle|\xi|\rangle(\xi \otimes \xi) dV_{x'} \tag{3}$$

where $\boldsymbol{K}$ is the shape tensor and $\omega\langle|\xi|\rangle = e^{-\left(\frac{\xi^2}{\delta^2}\right)}$ is the Gaussian influence function. Now, the strain tensor $(\boldsymbol{E})$ and the second Piola-Kirchhoff stress tensor $(\boldsymbol{S})$ at a material point x can be calculated using continuum mechanics[6] as

$$\boldsymbol{E} = \frac{1}{2}[\boldsymbol{F}^{\boldsymbol{T}}\boldsymbol{F} - \boldsymbol{I}] \tag{4}$$

$$\boldsymbol{S} = \boldsymbol{C} : \boldsymbol{E} \tag{5}$$

where $\boldsymbol{C}$ is the isotropic elastic moduli matrix and $\boldsymbol{I}$ is the identity matrix.

Finally, by constitutive correspondence, the force state can be obtained as

$$\boldsymbol{T}[\boldsymbol{x}]\langle\xi\rangle = \omega\langle|\xi|\rangle \boldsymbol{P}\boldsymbol{K}^{-1}\xi \tag{6}$$

where $\boldsymbol{P} = \boldsymbol{F}\boldsymbol{S}$ is the first Piola-Kirchhoff stress tensor. The force state calculated by Equation 6 was substituted into Equation 1 to solve the PD system.

3 CLASSICAL ELASTOPLASTIC CONSTITUTIVE MODEL

In this study, an elastoplastic constitutive model incorporating the von Mises yield criterion with strain softening was utilized to model geomaterials under plane strain compression. This model was selected because it provides a smooth and mathematically trackable framework for modelling plastic deformation in geomaterials when the focus is on distortional energy-driven failure mechanisms[17]. While traditional geotechnical criteria like Drucker-Prager account for pressure-dependent behavior, the von Mises approach is particularly suitable for simulating shear band initiation and propagation in cohesive soils under plane strain conditions, where the emphasis is on capturing the fundamental mechanics of strain localization[13, 17].

The strain tensor calculated using Equation 4 was decomposed into elastic and plastic parts, $\epsilon = \epsilon^e + \epsilon^p$. Plastic deformation is initiated when the stress state due to the total strain increment reaches the von Mises yield criterion given in Equation 7, triggering the plastic update procedure[13].

$$\Phi = \sqrt{3J_2\big(\eta(\boldsymbol{\sigma}, \boldsymbol{\beta})\big)} - \sigma_y \tag{7}$$

where $\boldsymbol{J_2} = \frac{1}{2}\boldsymbol{s} : \boldsymbol{s}$ is the second invariant of the stress tensor (σ), $\boldsymbol{s} = \boldsymbol{\sigma} - \frac{1}{3}tr(\boldsymbol{\sigma})\boldsymbol{I}$ is the deviatoric stress tensor, $\boldsymbol{I}$ is the identity tensor, $\boldsymbol{\eta} = \boldsymbol{s} - \boldsymbol{\beta}$ is the relative stress tensor, and $\boldsymbol{\beta}$ is the back stress tensor depends on the softening constant $(\boldsymbol{H})$ of the material given as

$$\boldsymbol{\beta} = \sqrt{\frac{2}{3}}\boldsymbol{H}\left(\frac{\boldsymbol{\eta}}{||\boldsymbol{\eta}||}\right) \tag{8}$$

While updating plastic strain, the equivalent plastic strain can be calculated as $\epsilon_{eq}^{pl} = \sqrt{\frac{2}{3}}|\epsilon^{pl}|$ to visualize the shear bands[12, 13].

Finally, the stress computed from the constitutive model can be used in Equation 6 to update the force state and subsequently applied in the peridynamic governing equation.

4 PERIDYNAMIC MODEL SETUP AND OPTIMIZATION

4.1 Numerical Model

To investigate the effect of microparameters on the elastic and plastic response and shear localization, plane strain compression tests were simulated using NOSB-PD. The geomaterial specimen of size $1\ m \times 2\ m$ was discretized into material points, with a displacement boundary condition applied at the top and a fixed boundary condition at the bottom using fictitious material points, as shown in red in Figure 2. The geomaterial properties used in PD simulations are presented in Table 1. Displacement rate $\dot{u} = 0.01\ m/s$ was applied to the top fictitious material points. To maintain the equilibrium, the time-step size was set to half the critical time-step, and an artificial damping coefficient $C = 5 \times 10^5\ kg/(m^3 s)$ was applied[12].

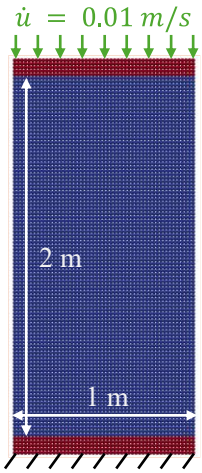

Figure 2: Numerical domain of the geomaterial specimen under plane strain compression

Table 1: Geomaterial properties

Material Parameters	Values
Young's modulus, E	50 MPa
Poisson's ratio, ν	0.3
Yield stress, σ_y	0.15 MPa
Softening modulus, H	1.5 MPa

4.2 Microparameter optimization

The accuracy and reliability of the peridynamic framework are fundamentally dependent on the proper calibration of key microparameters that govern the nonlocal interactions and numerical discretization[15]. Critical parameters, including horizon, material point discretization, and influence function selection, directly influence the computational accuracy of material elastic property predictions that ultimately affect the plastic response of geomaterials[1, 16]. This study evaluates the optimization of microparameters by the convergence of the average Young's modulus over all material points until it approaches the Young's modulus assigned at the individual material point level in the NOSB-PD framework.

Firstly, the material point discretization of the proposed model was verified. For this, the horizon size was fixed as $\delta = 0.08\,m$ and the number of material points in the horizon was varied such that the dimensionless parameter $m = horizon(\delta)/spacing(\Delta x)$ ranged from $1\ to\ 6$. The result presented in Figure 3(a) showed that for $m < 3$, the average Young's modulus was slightly higher than the target value and converged after $m \geq 4$.

From this convergence analysis, the configuration with 5151 material points and $0.02\,m$ spacing corresponding to $m = 4$ was selected to perform the horizon optimization. Subsequently, with the fixed material point configuration, the horizon size was varied to achieve m values ranging from $1\ to\ 6$. Figure 3(b) demonstrated consistent convergence

patterns, confirming the reliability of the microparameter optimization approach and verifying the selection of $m = 4$ for further implementation of the NOSB-PD framework.

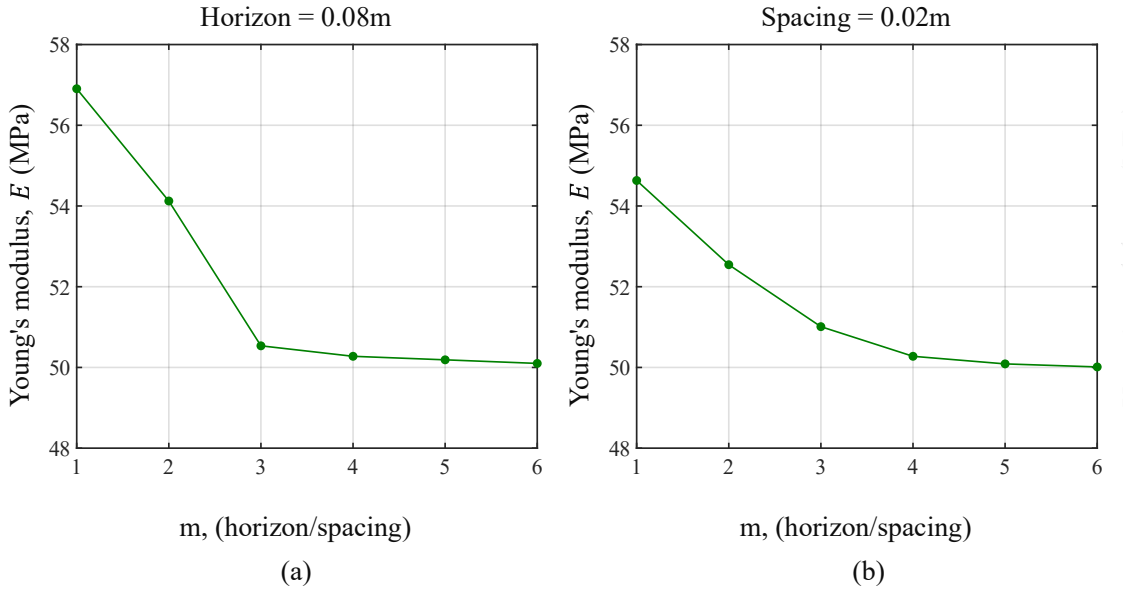

Figure 3: Convergence of Young's modulus by (a) Material points optimization and (b) Horizon optimization

5 RESULTS AND DISCUSSIONS

5.1 Elastoplastic response and shear localization in geomaterials

The elastoplastic behavior and material point optimization for shear localization in geomaterial were assessed by employing a similar convergence approach as the material point optimization. The analysis maintains a fixed horizon of $0.08\,m$ while increasing the particle density in the horizon to achieve $m = 1\ to\ 6$. This methodology enables the investigation of strain localization patterns and the quantification of shear band width. The shear band width was measured along a line oriented at $45°$ to the loading directions (extending from the coordinates $(0, 0.5)$ to $(1, 1.5)$) up to 1% strain to capture the onset and early development of localization phenomena.

The equivalent plastic strain contour maps at 1% strain level presented in Figure 4(a) reveal that the formation of distinctive X-shaped shear band patterns occurs at $45°$ to the loading directions. Under plane strain compression loading with the von Mises yield criterion, plastic deformation initiates along planes where the equivalent stress first exceeds the yield strength, which occurs at approximately $45°$ to the loading direction, consistent with the literature[13, 17]. The shear bands initiate from the corners of the specimen and gradually propagate from the bottom to the center of the specimen (at $45°$). This can be attributed to the confinement effect induced by the fixed boundary condition and application of the von Mises failure criterion to the NOSB-PD framework.

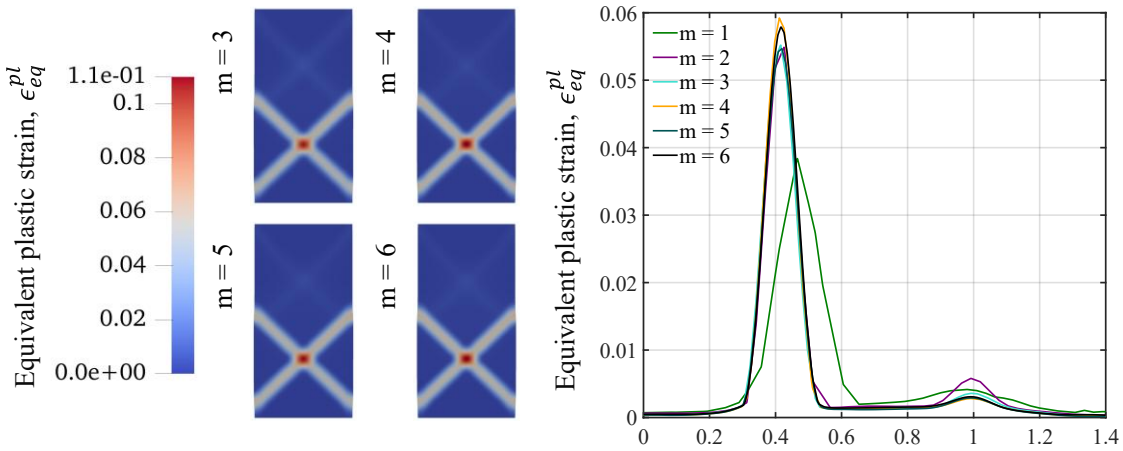

Equivalent plastic strain contour maps

(a)

(b)

Figure 4: (a) Equivalent plastic strain contour maps at 1% of strain, (b) Equivalent plastic strain along 45° line for varying m at 1% of strain

Figure 4(b) shows the equivalent plastic strain distribution along the measurement line at 1% strain level to quantify the material point density convergence of shear band formation observed in the contour maps by measuring the shear band width. The shear band width was defined as the distance between points where equivalent plastic strain drops to 10% of its peak value[12]. The results demonstrated that the material point density for $m = 1$ produces wider, diffused strain profiles with lower peak values and broader localization zones. This performance is due to sparse particle distribution within the horizon, which limits accurate deformation gradient calculation and restricts diagonal interactions necessary for proper shear deformation capture[12]. Therefore, optimal discretization is required for adequate particle connectivity that enables capturing sharp shear localization. For $m = 2\ to\ 6$, the shear band width narrows substantially, and peak strain values stabilize, which shows the discretization-independent behavior.

Based on a comprehensive convergence study for elastic modulus and shear band width, the optimal discretization parameters of $m = 4, \delta = 0.08\ m, and\ \Delta x = 0.02\ m$ provides a reliable and resolution-independent prediction of shear localization behavior, forming a foundation for realistic loading condition simulations.

5.2 Shear band evolution in geomaterials

Figure 5 illustrates the evolution of shear band development through equivalent plastic strain contours at strain levels of 1 %, 1.3 %, and 1.6 %. At the strain level of 1 %, the formation of conjugate shear bands is evident, with plastic deformation initiating along diagonal planes oriented at approximately 45° to the loading direction. As strain increases to 1.3 %, a transition begins to occur with preferential plastic strain concentrations developing along one diagonal direction. Subsequently, a distinct critical zone with plastic strain of 0.3 was observed at a strain level of 1.6 % leading to shear failure. This behavior can be attributed to the non-uniform response of the NOSB-PD framework due to the development of higher plastic strain, which

will be investigated in future studies.

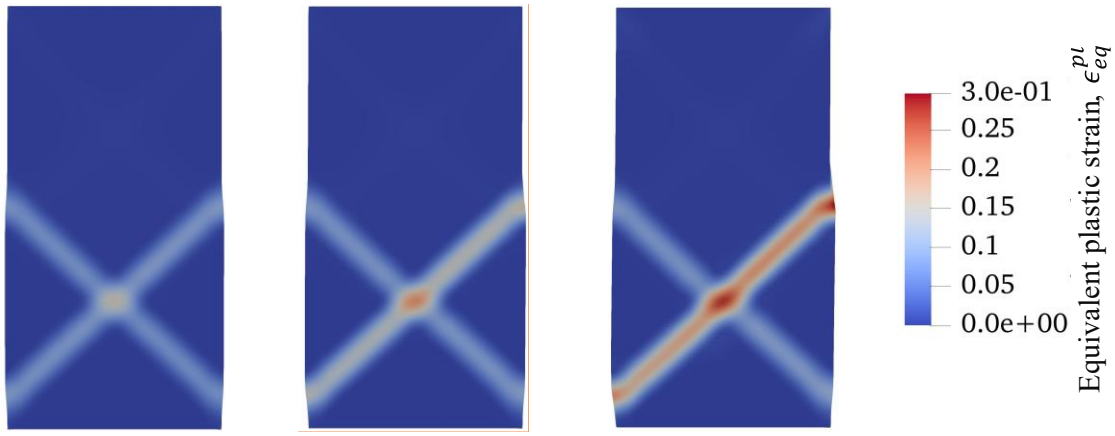

Figure 5: Shear band evolution with $m = 4$ and $\delta = 0.08$

6 CONCLUSIONS

This study investigates the optimization of peridynamic microparameters for accurate representation of elasticity, plasticity, and shear localization in geomaterials under plane strain compression loading conditions. NOSB-PD formulation with von Mises plasticity was utilized to employ systematic convergence analysis to establish optimal discretization parameters for reliable strain localization prediction. The key findings of this study can be summarized as follows:

- The convergence analysis identified the optimal discretization parameter as $m = 4$ to ensure accurate elastic response while maintaining computational efficiency.
- The peridynamic formulation captured the conjugate shear band formation at 45° orientations consistent with the von Mises yield criterion and effectively reproduced evolution from distributed conjugate failure to localized single-band failure.

REFERENCES

[1] X. Song and N. Khalili, "A peridynamics model for strain localization analysis of geomaterials," *Int. J. Numer. Anal. Methods Geomech.*, vol. 43, no. 1, pp. 77–96, Jan. 2019, doi: 10.1002/nag.2854.

[2] H. Yan, A. P. Jivkov, and M. Sedighi, "Modelling soil desiccation cracking by peridynamics," *Geotechnique*, vol. 73, no. 5, pp. 388–400, 2023, doi: 10.1680/jgeot.21.00032.

[3] C. E. Augarde, S. J. Lee, and D. Loukidis, "Numerical modelling of large deformation problems in geotechnical engineering: A state-of-the-art review," *Soils Found.*, vol. 61, no. 6, pp. 1718–1735, Dec. 2021, doi: 10.1016/j.sandf.2021.08.007.

[4] S. A. Silling, "Reformulation of elasticity theory for discontinuities and long-range forces," *J. Mech. Phys. Solids*, vol. 48, no. 1, pp. 175–209, 2000, doi: 10.1016/S0022-5096(99)00029-0.

[5] S. A. Silling, M. Epton, O. Weckner, J. Xu, and E. Askari, *Peridynamic states and constitutive modeling*, vol. 88, no. 2. 2007. doi: 10.1007/s10659-007-9125-1.
[6] P. Li, Z. M. Hao, and W. Q. Zhen, "A stabilized non-ordinary state-based peridynamic model," *Comput. Methods Appl. Mech. Eng.*, vol. 339, pp. 262–280, 2018, doi: 10.1016/j.cma.2018.05.002.
[7] X.-P. Zhou and Y.-T. Wang, "State-of-the-Art Review on the Progressive Failure Characteristics of Geomaterials in Peridynamic Theory," *J. Eng. Mech.*, vol. 147, no. 1, pp. 1–18, 2021, doi: 10.1061/(asce)em.1943-7889.0001876.
[8] C. O'Sullivan, "Particle-Based Discrete Element Modeling: Geomechanics Perspective," *Int. J. Geomech.*, vol. 11, no. 6, pp. 449–464, 2011, doi: 10.1061/(asce)gm.1943-5622.0000024.
[9] D. Bhattacharya, M. Mukherjee, and A. Prashant, "Perturbation Intensity and Mesh Convergence in Coupled Undrained Instability Analysis in Sands under Biaxial Loading," *Int. J. Geomech.*, vol. 20, no. 7, pp. 1–14, 2020, doi: 10.1061/(asce)gm.1943-5622.0001694.
[10] P. V. Satheesh, D. Shirole, and S. Sinha, "Investigation of the Effect of Confinement on Intact Wombeyan Marble Using Continuum Grain-Based Model (CGBM)," *58th US Rock Mech. / Geomech. Symp. 2024, ARMA 2024*, no. June, 2024, doi: 10.56952/ARMA-2024-0310.
[11] C. Wang, J. Zhao, and W. Zheng, "Progressive Failure Analysis of Soil Slope with Strain Softening Behavior Based on Peridynamics," *Adv. Civ. Eng.*, vol. 2023, 2023, doi: 10.1155/2023/6816673.
[12] H. Zhou, F. Shen, X. Gu, and B. Li, "Regularization effect of peridynamic horizon on strain localization and soil slope instability analysis," *Eng. Anal. Bound. Elem.*, vol. 165, no. May, p. 105774, 2024, doi: 10.1016/j.enganabound.2024.105774.
[13] E. A. De Souza Neto, D. Perić, and D. R. J. Owen, *Computational Methods for Plasticity: Theory and Applications*. 2008. doi: 10.1002/9780470694626.
[14] F. Bobaru, M. Yang, L. F. Alves, S. A. Silling, E. Askari, and J. Xu, "Convergence, adaptive refinement, and scaling in 1D peridynamics," *Int. J. Numer. Methods Eng.*, vol. 77, no. 6, pp. 852–877, Feb. 2009, doi: 10.1002/nme.2439.
[15] W. Liu and J. W. Hong, "Discretized peridynamics for linear elastic solids," *Comput. Mech.*, vol. 50, no. 5, pp. 579–590, 2012, doi: 10.1007/s00466-012-0690-1.
[16] S. Menon and X. Song, "Shear banding in unsaturated geomaterials through a strong nonlocal hydromechanical model," *Eur. J. Environ. Civ. Eng.*, vol. 26, no. 8, pp. 3357–3371, 2022, doi: 10.1080/19648189.2020.1797889.
[17] N. Bordignon, A. Piccolroaz, F. Dal Corso, and D. Bigoni, "Strain localization and shear band propagation in ductile materials," *Front. Mater.*, vol. 2, no. March, pp. 1–13, 2015, doi: 10.3389/fmats.2015.00022.